

1 **Structural basis for potent neutralization of SARS-CoV-2 and role of antibody affinity**

2 **maturation**

3

4 Nicholas K. Hurlburt¹, Yu-Hsin Wan¹, Andrew B. Stuart¹, Junli Feng¹, Andrew T. McGuire^{1,2}, Leonidas

5 Stamatatos^{1,2}, Marie Pancera^{1,3}

6

7 ¹Fred Hutchinson Cancer Research Center, Vaccines and Infectious Diseases Division, Seattle, WA, USA

8 ²University of Washington, Department of Global Health, Seattle, WA, USA

9 ³Vaccine Research Center, National Institutes of Allergy and Infectious Diseases, National Institute of

10 Health, Bethesda, MD, USA

11 Correspondence: mpancera@fredhutch.org

12

13 **Abstract**

14 SARS-CoV-2 is a betacoronavirus virus responsible for the COVID-19 pandemic. Here, we determined the

15 X-ray crystal structure of a potent neutralizing monoclonal antibody, CV30, isolated from a patient

16 infected with SARS-CoV-2, in complex with the receptor binding domain (RBD). The structure reveals

17 CV30's epitope overlaps with the human ACE2 receptor binding site thus providing the structural basis

18 for its neutralization by preventing ACE2 binding.

19

20

21 **Main**

22 COVID-19 was declared a pandemic in March 2020 by the World Health Organization¹. As of June 11th,
23 2020, there were ~ 7.4 M infections and over 415,000 deaths worldwide². It is caused by a coronavirus
24 of the beta family, named SARS-CoV-2³, as it is closely related to SARS-CoV⁴. Their genomes share 80%
25 identity and they utilize angiotensin-converting enzyme 2 (ACE2) as receptor for entry⁵⁻¹¹. Viral entry
26 depends on the SARS-CoV-2 spike glycoprotein, a class I fusion protein comprised of two subunits, S1
27 and S2. S1 mediates ACE2 binding through the receptor binding domain (RBD), while the S2 subunit
28 mediates fusion. Overall the spike shares 76% amino acid sequence homology with SARS⁴. High
29 resolutions structures of the SARS-CoV-2 stabilized spike in the prefusion revealed that the RBD can be
30 seen in a 'up' or 'down' conformation^{5,6}. It's been shown that some of the neutralizing antibodies bind
31 the RBD in the 'up' conformation similar to when the ACE2 receptor binds¹². Currently there is no
32 vaccine available to prevent SARS-CoV-2 infection and highly effective therapeutics have not been
33 developed yet either. The host immune response to this new coronavirus is also not well understood.
34 We, and others, sought to characterize the humoral immune response from infected COVID-19
35 patients¹²⁻¹⁴. Recently, we isolated a neutralizing antibody, named CV30, which binds the receptor
36 binding domain (RBD), neutralizes with 0.03 µg/ml and competes binding with ACE2¹⁵. However, the
37 molecular mechanism by which CV30 blocked ACE2 binding was unknown. Herein, we present the 2.75
38 Å crystal structure of SARS-CoV-2 RBD in complex with the Fab of CV30 (Extended Data Table 1).

39

40 CV30 binds almost exclusively to the concave ACE2 binding epitope (also known as the receptor binding
41 motif (RBM)) of the RBD using all six CDR loops with a total buried surface area of ~1004 Å², ~750 Å²
42 from the heavy chain and ~254 Å² from the kappa chain (Fig. 1A). 20 residues from heavy chains and 10
43 residues from the kappa chain interact with the RBD, forming 13 and 2 hydrogen bonds, respectively

44 (Fig. 1C and Extended Data Table 2). There are 29 residues from the RBD that interact with CV30, 19
45 residues with the heavy chain, 7 residues with the light chain, and 3 residues with both (Extended Data
46 Table 2). Of the 29 interacting residues from the SARS-CoV-2 RBD, only 16 are conserved in the SARS-
47 CoV S protein RBD (Fig. 2c), which could explain the lack of cross-reactivity of CV30 to SARS-CoV S¹⁵. The
48 CV30 heavy chain is minimally mutated with only a two-residue change from the germline and both of
49 these residues (Val27-Ile28) are located in the CDRH1 and form nonpolar interactions with the RBD. We
50 reverted these residues to germline to assess their role. Interestingly, the germline CV30 (gICV30)
51 antibody bound to RBD with ~100-fold lower affinity (407 nM affinity) (Fig 1d and Extended Data Table
52 3) compared to CV30 (3.6 nM¹⁵) with a very large difference in the off-rate. gICV30 neutralized SARS-
53 CoV-2 with ~500-fold difference with an IC50 of 16.5 vs 0.03 µg/mL for CV30 (Fig. 1e). Val27 forms a
54 weak non-polar interaction with the RBD Asn487 and sits in a pocket formed by CDRH1 and 3. Although
55 it is unclear, Phe27 presents in gICV30 could change the electrostatic environment. The Ile28 sidechain
56 forms non-polar interactions with the RBD Gly476-Ser447, particularly the Cy atom, which the gICV30
57 Thr would be incapable of making. Thus, minimal affinity maturation of CV30 significantly impacted the
58 ability of this mAb to neutralize SARS-CoV-2.

59

60 CV30 competes with ACE2 for binding to the RBD¹⁵ and we therefore examined the structural
61 mechanism of the receptor blocking by superimposing the SARS-CoV-2 RBD/ACE2 complex (PDB: 6LZG)⁹
62 with the CV30 Fab/RBD complex. The structure of the RBD was used to align the two complexes and
63 showed that CV30 binding did not induce any conformational changes in the RBD from the ACE2-bound
64 complex. The aligned RBD had a RMSD of 0.353 Å over 166 C_α atoms. The structure reveals that the
65 CV30 epitope overlaps almost completely with the ACE2 epitope. A total of 26 residues of the SARS-CoV-
66 2 RBD interact with hACE2, CV30 binds to 19 of these residues (Fig. 2A), indicating that CV30 neutralizes
67 the virus by preventing the binding of ACE2 to RBD by direct steric interactions.

68

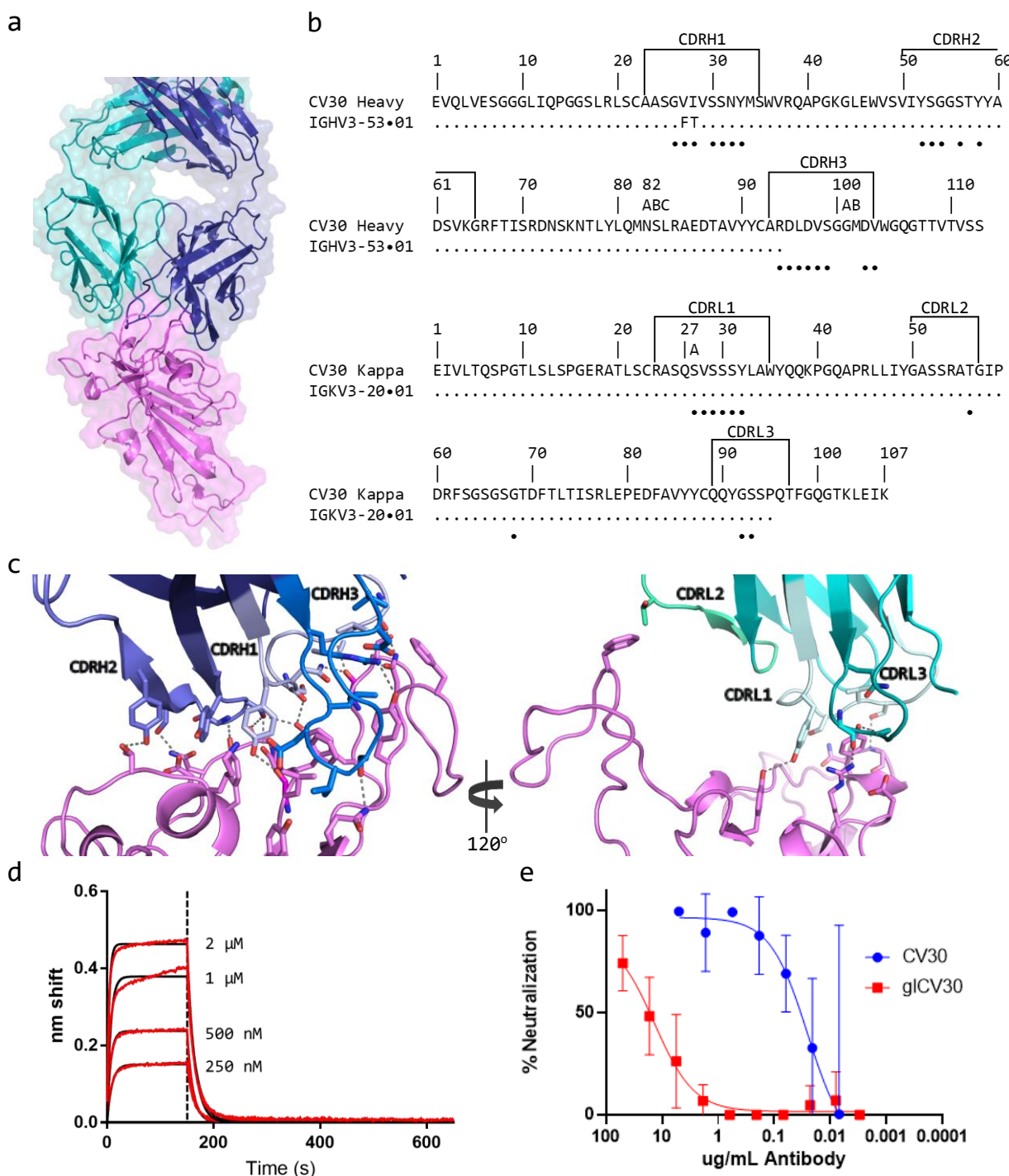
69 Recently, the structure of two potent neutralizing anti-RBD antibodies were published, B38 and CB6^{12,14}.
70 CV30 shares a similar germline heavy chain V-genes but all three have diverse germline kappa V-genes
71 (CV30 is IGKV3-20*01, B38 is IGKV1-9*01, CB6 is IGKV1-39*01, Extended Data Fig. 1). Both CV30 and
72 B38 use IGHV3-53*01 while CB6 uses IGHV3-66*01, which is only one amino acid different than 3-53*01
73 (Val12 which does not make contact with the epitope). CV30 and CB6 each have higher affinities, 3.6 nM
74 and 2.5 nM, respectively, than B38, 70.1 nM^{12,14,15}. Differences in affinity translate into differences in
75 neutralization potency (the IC50s for CV30 and CB6 are 0.03 and 0.036 µg/mL, respectively, and that of
76 B38 is 0.177 µg/mL). Interestingly, Thr28 was also mutated from germline to Ile in B38 but Phe27 was
77 not. CB6 lacks both mutations found in CV30. Differences in other regions of the antibody, such as the
78 CDRH3 and light chain are likely responsible for the overall potency all these antibodies (see below). To
79 investigate the binding mechanism of the three antibodies, a superposition of the structures was
80 created. All three bind in a nearly identical manner with the same angle of approach and similar
81 footprints (Fig. 2b). The alignment of the Fv regions of B38 and CB6 to the Fv region of CV30 had a RMSD
82 of 0.240 Å over 100 C_α atoms and 0.329 Å over 98 C_α atoms, respectively. Mapping the binding
83 interactions of the RBD to each of the antibodies reveals a close overlap in the binding mechanism (Fig.
84 2c-d). The footprint of the heavy chain is nearly identical, as expected from the shared germline V-gene
85 and sequence similarity. CV30 and CB6 both have longer CDRH3 and bind with higher buried surface
86 area, ~263 and ~251 Å², respectively, than B38 (~203 Å²) (Fig. 2d, Extended Data Fig. 1). The large
87 difference is in the light chain. CV30 has the smallest binding interaction at ~254 Å², B38 has the largest
88 interaction at ~497 Å² and then CB6 at ~354 Å². One of the more interesting findings was the interaction
89 of Thr56 in the CV30 CDRK2 which reaches across the RBD and interacts Phe486, an interaction that is
90 not found in the other two antibodies (Extended Data Fig. 1).

91

92 In conclusion, our structure indicates that potent neutralizing antibodies against SARS-CoV-2 bind the
93 receptor binding motif in the RBD, overlapping the ACE2 binding site, but recognize residues that are
94 specific for SARS-CoV-2 only, thus explaining the lack of cross neutralization with SARS-CoV. It is
95 noteworthy that potently neutralizing antibodies isolated from multiple individuals use the same or
96 similar VH gene to target their epitope. Additionally, the minimal affinity maturation observed 21 days
97 after infection in the VH gene of CV30 showed ~100-500-fold increase in affinity and neutralization
98 potency, indicating that further affinity maturation may increase potency and potential cross-reactivity.
99 Our studies indicate that the RBD is a promising target for vaccine design and that these potently
100 neutralizing antibodies should be explored as a treatment for COVID-19 infection.

101

102 **Figure legends**



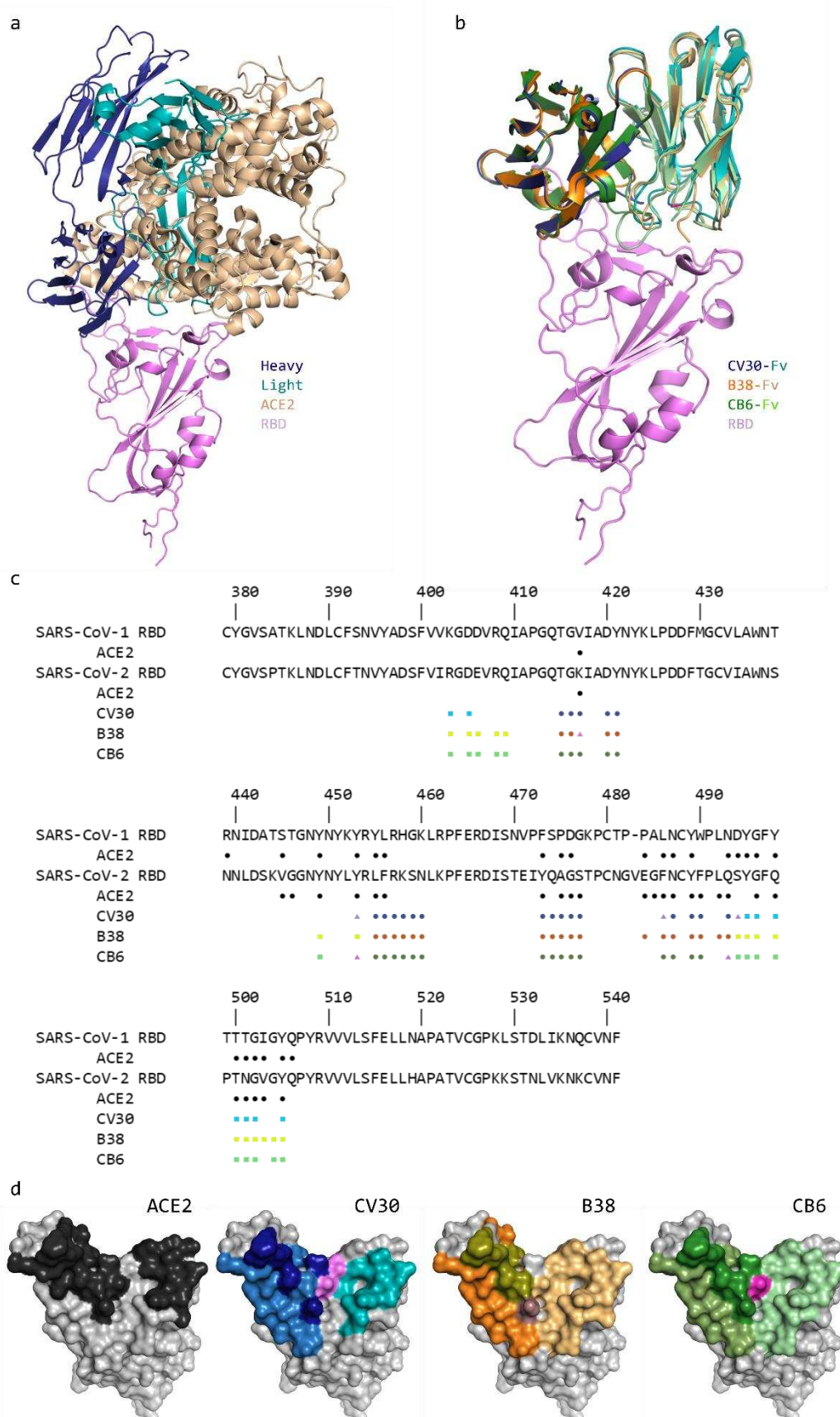
103

104 **Figure 1. Overall structure of CV30 Fab in complex with SARS-CoV-2 RBD and kinetics of gICV30. a.**

105 Structure is shown in cartoon with surface representation shown in transparency. CV30 heavy chain is

106 shown in dark blue and light chain in light blue. RBD is shown in pink. **b.** Sequence alignment of CV30
107 heavy and light chains with germline genes. Black circles underneath the sequence indicate residues that
108 interact with the RBD. **c.** Details of the interactions of the heavy (left) and light (right) chains with the
109 RBD. CDRs are labeled and colored as shown. Residues that interacts are shown as sticks and Hydrogen
110 bonds are shown in dotted lines. **d.** Kinetics of gICV30 binding to RBD measured by BLI. **e.** gICV30 and
111 CV30 neutralization of SARS-CoV-2 pseudovirus.

112



114 **Figure 2. Comparison of the CV30 epitope against ACE2 and other neutralizing antibodies. a.** Structural
115 overlay of ACE2/RBD complex with CV30/RBD complex. **b.** Structural alignment of the variable domains
116 of CV30, B38, and CB6. **c.** Sequence alignment of SARS-CoV RBD and SARS-CoV-2 RBD. The residues that
117 interact with ACE2 are indicated by the black circles. Residues that interact with CV30, B38, and CB6 are
118 indicated by the colored squares (light chain interactions), circles (heavy chain interactions), or triangles
119 (interactions with both chains). **d.** Surface representation of the RBD with the binding epitope colored.
120 Light chain interactions are the lightest color, heavy chain interactions are next lightest, and CDRH3
121 specific interactions are darkest, and interacting with both heavy and light chain is purple.

122

123 **Methods**

124 **Recombinant Protein Expression and Purification**

125 The plasmid encoding the receptor binding domain of SARS-CoV-2 spike protein fused to a monomeric
126 Fc (pαH-RBD-Fc) has been previously described⁵ and was a gift from Dr. Jason McLellan.
127 1L of 293SGlycoDelete cells¹⁶ were cultured to a density of 1 million cells/mL and transiently transfected
128 with 500μg of pαH-RBD-Fc using 2 mg of polyethylenimine (PEI, Polysciences, Cat# 24765). Cultural
129 supernatant was harvested 6 days post-transfection by centrifugation and sterile filtered using a 0.22μm
130 vacuum filter. The RBD was purified using protein A agarose resin (GoldBio, Cat# P-400) and cleaving the
131 Fc domain using HRV3C protease (made in house) on-column. The eluate containing the RBD was further
132 purified by SEC using a HiLoad 16/600 Superdex 200 pg column (GE Healthcare) column pre-equilibrated
133 in 2mM Tris-HCl, pH 8.0, 200mM NaCl. Protein was aliquoted, flash frozen, and stored at -80°C until
134 needed.

135

136 500mL of 293EBNA cells were cultured to a density of 1 million cells/mL and transiently transfected with
137 125µg each of CV30 Heavy and Kappa chains using 1 mg of PEI. Cultural supernatant was harvested 6
138 days post-transfection by centrifugation and sterile filtered using a 0.22µm vacuum filter. IgG was
139 purified using protein A agarose resin and eluted using Pierce IgG Elution Buffer (Thermo Scientific, Cat#
140 21004). Eluate was pH adjusted to 7.5 using 1M HEPES, pH 7.5. IgG was further purified by SEC using a
141 HiLoad 16/600 Superdex 200 pg column. Antigen binding fragment (Fab) was generated by incubating
142 IgG with LysC (New England Biolabs, Cat# P8109S) at a ratio of 1µg LysC per 10mg IgG at 37°C for 18hrs.
143 Fab unexpectedly stuck to protein A resin and was eluted as mixture of Fab, undigested IgG, and
144 digested Fc product using the IgG elution buffer. Fab and Fc product was purified by SEC. The CV30-Fab
145 and SARS-CoV-2 RBD complex was obtained my mixing Fab and Fc product with a 2-fold molar excess of
146 RBD and incubated for 90min at RT with nutation followed by SEC. The complex was verified by SDS-
147 PAGE analysis.

148

149 **Crystal Screening and Structure Determination**

150 The complex was concentrated to 10mg/mL for initial crystal screening by sitting-drop vapor-diffusion in
151 the MCG Suite (Anatrace) using a NT8 drop setter (Formulatrix). Diffracting crystals were obtained in a
152 mother liquor (ML) containing 0.2M (NH₄) Citrate, tribasic, pH 7.0 and 12% (w/v) PEG 3350. The crystals
153 were cryoprotected by soaking in ML supplemented with 30% (v/v) ethylene glycol. Diffraction data was
154 collected at Advanced Photon Source (APS) SBC 19-ID at a 12.662 keV. The data set was processed using
155 XDS¹⁷ to a resolution of 2.75Å. The structure of the complex was solved by molecular replacement using
156 Phaser¹⁸ with a search model of SARS-CoV-2 RBD (PDBid: 6lzg)¹⁹ and the Fab structure (PDBid: 5i1e)¹⁹
157 divided into Fv and Fc portions. Remaining model building was completed using COOT²⁰ and refinement

158 was performed in Phenix²¹. The data collection and refinement statistics are summarized in Extended
159 Data Table 1. Structural figures were made in Pymol.

160 **BLI**

161 For kinetic analyses gICV30 was captured on anti-Human IgG Fc capture (AHC) sensors at a
162 concentration of 20 µg/mL and loaded for 100s. After loading, the baseline signal was then recorded for
163 1min in KB. The sensors were immersed into wells containing serial dilutions of purified SARS-CoV-2 RBD
164 in KB for 150s (association phase), followed by immersion in KB for an additional 600s (dissociation
165 phase). The background signal from each analyte-containing well was measured using VRC01 IgG control
166 reference sensors and subtracted from the signal obtained with each corresponding gICV30 loaded
167 sensor. Kinetic analyses were performed at least twice with an independently prepared analyte dilution
168 series. Curve fitting was performed using a 1:1 binding model and the ForteBio data analysis software.
169 Mean kon, koff values were determined by averaging all binding curves that matched the theoretical fit
170 with an R2 value of ≥0.98.

171 **Neutralization Assay**

172 HIV-1 derived viral particles were pseudotyped with full length wildtype SARS-CoV-2 S²². Briefly,
173 plasmids expressing the HIV-1 Gag and pol (pHDM540 Hgpm2), HIV-1Rev (pRC-CMV-rev1b), HIV-1 Tat
174 (pHDM-tat1b), the SARS-CoV-2 spike (pHDM-SARS-CoV-2 Spike) and a luciferase/GFP reporter (pHAGE-
175 CMV-Luc2-IRES542 ZsGreen-W) were co-transfected into 293T cells at a 1:1:1:1.6:4.6 ratio using 293
176 Free transfection reagent according to the manufacturer's instructions. 72 hours later the culture
177 supernatant was harvested, clarified by centrifugation and frozen at -80°C.

178 293 cells stably expressing ACE2 (HEK-293T-hACE2) were seeded at a density of 4x10³ cells/well in a 100
179 µL volume in 96 well flat bottom tissue culture plates. The next day, CV30 and germline CV30 were
180 serially diluted in 30 µL of cDMEM in 96 well round bottom 27 plates in triplicate. An equal volume of

181 viral supernatant diluted to result in 2×10^5 luciferase units was added to each well and incubated for 60
182 min at 37 °C. Meanwhile 50 µL of cDMEM containing 6 µg/mL polybrene was added to each well of
183 293T-ACE2 cells (2 µg/mL final concentration) and incubated for 30 min. The media was aspirated from
184 293T-ACE2 cells and 100 µL of the virus-antibody mixture was added. The plates were incubated at 37°C
185 for 72 hours. The supernatant was aspirated and replaced with 100 µL of Steadyglo luciferase reagent
186 (Promega). 75 µL was then transferred to an opaque, white bottom plate and read on a Fluorskan
187 Ascent Fluorimeter. Control wells containing virus but no antibody (cells + virus) and no virus or
188 antibody (cells only) were included on each plate.

189 % neutralization for each well was calculated as the RLU of the average of the cells + virus wells, minus
190 test wells (cells +mAb + virus), and dividing this result difference by the average RLU between virus
191 control (cells+ virus) and average RLU between wells containing cells alone, multiplied by 100. The
192 antibody concentration that neutralized 50% of infectivity (IC50) was interpolated from the
193 neutralization curves determined using the log(inhibitor) vs. response -- Variable slope (four
194 parameters) fit using automatic outlier detection in Graphpad Prism Software.

195

196 **Data availability**

197 Coordinates and structure factors for CV30 Fab-SARS-CoV-2 RBD complex have been deposited in the
198 Protein Data Bank (PDB) under the accession code 6XE1.

199

200 **References**

- 201 1. Mahase, E. Covid-19: WHO declares pandemic because of "alarming levels" of spread, severity,
202 and inaction. *BMJ* **368**, m1036 (2020).
- 203 2. Dong, E., Du, H. & Gardner, L. An interactive web-based dashboard to track COVID-19 in real
204 time. *Lancet Infect Dis* (2020).

205 3. Wu, Y. et al. SARS-CoV-2 is an appropriate name for the new coronavirus. *Lancet* (2020).

206 4. Wan, Y., Shang, J., Graham, R., Baric, R.S. & Li, F. Receptor Recognition by the Novel Coronavirus
207 from Wuhan: an Analysis Based on Decade-Long Structural Studies of SARS Coronavirus. *J Virol*
208 **94**(2020).

209 5. Wrapp, D. et al. Cryo-EM structure of the 2019-nCoV spike in the prefusion conformation.
210 *Science* **367**, 1260-1263 (2020).

211 6. Walls, A.C. et al. Structure, Function, and Antigenicity of the SARS-CoV-2 Spike Glycoprotein. *Cell*
212 (2020).

213 7. Hoffmann, M. et al. SARS-CoV-2 Cell Entry Depends on ACE2 and TMPRSS2 and Is Blocked by a
214 Clinically Proven Protease Inhibitor. *Cell* (2020).

215 8. Yan, R. et al. Structural basis for the recognition of SARS-CoV-2 by full-length human ACE2.
216 *Science* **367**, 1444-1448 (2020).

217 9. Wang, Q. et al. Structural and Functional Basis of SARS-CoV-2 Entry by Using Human ACE2. *Cell*
218 (2020).

219 10. Letko, M., Marzi, A. & Munster, V. Functional assessment of cell entry and receptor usage for
220 SARS-CoV-2 and other lineage B betacoronaviruses. *Nat Microbiol* **5**, 562-569 (2020).

221 11. Ou, X. et al. Characterization of spike glycoprotein of SARS-CoV-2 on virus entry and its immune
222 cross-reactivity with SARS-CoV. *Nat Commun* **11**, 1620 (2020).

223 12. Shi, R. et al. A human neutralizing antibody targets the receptor binding site of SARS-CoV-2.
224 *Nature* (2020).

225 13. Ju, B. et al. Human neutralizing antibodies elicited by SARS-CoV-2 infection. *Nature* (2020).

226 14. Wu, Y. et al. A noncompeting pair of human neutralizing antibodies block COVID-19 virus binding
227 to its receptor ACE2. *Science* (2020).

228 15. Seydoux, E. et al. Analysis of a SARS-CoV-2 infected individual reveals development of potent
229 neutralizing antibodies to distinct epitopes with limited somatic mutation. *Immunity* (2020).

230 16. Meuris, L. et al. GlycoDelete engineering of mammalian cells simplifies N-glycosylation of
231 recombinant proteins. *Nat Biotechnol* **32**, 485-9 (2014).

232 17. Kabsch, W. Xds. *Acta Crystallogr D Biol Crystallogr* **66**, 125-32 (2010).

233 18. McCoy, A.J. et al. Phaser crystallographic software. *J Appl Crystallogr* **40**, 658-674 (2007).

234 19. Teplyakov, A. et al. Structural diversity in a human antibody germline library. *MAbs* **8**, 1045-63
235 (2016).

236 20. Emsley, P. & Cowtan, K. Coot: model-building tools for molecular graphics. *Acta Crystallogr D
237 Biol Crystallogr* **60**, 2126-32 (2004).

238 21. Adams, P.D. et al. Recent developments in the PHENIX software for automated crystallographic
239 structure determination. *J Synchrotron Radiat* **11**, 53-5 (2004).

240 22. Crawford, K.H.D. et al. Protocol and Reagents for Pseudotyping Lentiviral Particles with SARS-
241 CoV-2 Spike Protein for Neutralization Assays. *Viruses* **12**(2020).

242

243

244

245

246 **Acknowledgments**

247 This work was supported by generous donations to Fred Hutch COVID-19 Research Fund. We thank Dr.
248 McLellan for providing the SARS-CoV-2 RBD plasmid. We thank the J. B. Pendleton Charitable Trust for
249 its generous support of Formulatrix robotic instruments. Results shown in this report are derived from
250 work performed at Argonne National Laboratory, Structural Biology Center (SBC), ID-19, at the Advanced
251 Photon Source. SBC-CAT is operated by UChicago Argonne, LLC, for the U.S. Department of Energy,
252 Office of Biological and Environmental Research under contract DE-AC02-06CH11357.

253

254 **Author contribution**

255 N.K.H, A.T.M., L.S and M.P. conceived the project. N.K.H, A.T.M., L.S and M.P designed the experiments.
256 J.F. cloned the plasmids. N.K.H and A.B.S. expressed and purified the proteins. N.K.H. crystallized
257 proteins, collected and processed the diffraction data, and solved the crystal structure. N.K.H and A.J.M.
258 performed kinetic experiments. Y-H. W. and A.J.M performed neutralization assay. N.K.H, A.T.M., L.S
259 and M.P. analyzed and discussed data. N.K.H and M.P. wrote the original manuscript draft. N.K.H,
260 A.T.M., L.S and M.P. reviewed and edited the manuscript.

261